Retrobulbar Structure Visualization With Enhanced Depth Imaging Optical Coherence Tomography

Alessandro Invernizzi, Andrea Giani, Mario Cigada, and Giovanni Staurenghi

Eye Clinic, Department of Biomedical and Clinical Science, Luigi Sacco Hospital, University of Milan, Milan, Italy

Correspondence: Giovanni Staurenghi, Eye Clinic, Luigi Sacco Hospital, University of Milan, Via G.B. Grassi, 74-20157 Milan, Italy; giovanni.staurenghi@unimi.it.

Submitted: August 17, 2012
Accepted: March 13, 2013

Citation: Invernizzi A, Giani A, Cigada M, Staurenghi G. Retrobulbar structure visualization with enhanced depth imaging optical coherence tomography. *Invest Ophthalmol Vis Sci*. 2013;54:2678–2684. DOI: 10.1167/iovs.12-10786

Purpose. To assess enhanced depth imaging optical coherence tomography (EDI-OCT) visualization of deep posterior pole structures and retrobulbar tissues in myopic eyes and evaluate ocular structural elements that influence this capability.

Methods. Thirty consecutive myopic eyes (>−6 diopters) from 21 patients were enrolled. Exclusion criteria included any pathological condition affecting the posterior pole. Patients underwent biometry to assess axial length, and irises were classified as darkly or lightly pigmented. EDI-OCT scans were obtained by spectral-domain OCT to image posterior pole and retrobulbar structures. Choroidal thickness was measured manually, and for eyes in which the sclera was fully visible, scleral thickness was also measured manually. The influence of central retinal thickness, axial length, refractive error, mean choroidal thickness, mean scleral thickness, and iris pigmentation on EDI-OCT visualization of structures beyond the choroid was tested.

Results. Choroidal thickness was measurable in all eyes. In 11 of 30 eyes, the sclera was not completely visible (group 1). In 19 eyes, the full scleral thickness was measurable (group 2). In seven of the group 2 eyes, the full sclera was the deepest structure detected. In the remaining 11 eyes, deeper structures were visible. Choroidal thickness was the only parameter that correlated with the ability to visualize the full sclera ($P < 0.001$) and deeper structures ($P = 0.044$).

Conclusions. The full thickness of the choroid was visualized by EDI-OCT in all eyes. Full thicknesses of the sclera and retrobulbar structures were not always visible. Choroidal thickness was the only parameter that significantly correlated with EDI-OCT visualization of deeper structures.

Keywords: EDI-OCT, retrobulbar, myopia

Optical coherence tomography (OCT) is one of the most often used imaging techniques in ophthalmology. The capability to detect small alterations of retinal structure, especially at the posterior pole, makes it essential in the diagnostic process and in patient follow-up.[1] Since the introduction of OCT into clinical practice, the interest of ophthalmologists has been focused on the visualization of the retina.[2] For this reason, all of the currently available commercial instruments, especially the most recent high-resolution spectral-domain models, have the capability of collecting detailed images of the retina. In contrast, they are less efficient at acquiring information on other structures such as the choroid, sclera, or vitreous. In fact, these tissues need instruments with different technical characteristics for better visualization. For instance, the best way to image the structures lying above the retina, especially the vitreous body, is to employ OCT instruments with gold-plated mirrors.[3] However, these instruments are very expensive and available for research only. Imaging of deeper structures can be achieved with lasers of different wavelengths.[4] In particular, 1080-nm wavelength OCT instruments better visualize the deep structures of the eye (i.e., the choroid).[5] The major wavelength of these instruments, compared with standard near-infrared wavelengths used in normal OCT, can easily pass through the superficial layers and reach the tissues beyond.[4,5] Unfortunately the longer wavelengths of these instruments are less efficient in imaging the retinal tissue, thus they are inconvenient for clinical practice.

In the last few years a new imaging technique called "enhanced depth imaging" (EDI) has been developed to improve the capability of commercial spectral-domain OCT in collecting images of the deeper ocular structures.[6] The images are generated by analysis of the Fourier-transformed light signal sent through the retina. With this technique, each real image collected by the instrument is always accompanied by an EDI-inverted one. Commercial OCT instruments generally show the direct image in which the details decrease from the inner to the outer layers of the retina. For technical reasons,[6] the inverted image shows the greatest detail in the outer retina. Consequently, the deep structures are visualized in great detail.

Since EDI-OCT was introduced into clinical practice, it has played an important role in the study of the choroid and the sclera in health and disease.[7–9] Currently, EDI-OCT is proposed for the assessment of changes in choroidal thickness for pathological entities that mainly result in choroiditis such as occurs in Vogt-Koyanagi-Harada disease.[10] Additionally, even when vision loss occurs due to retinal alterations, the choroid and deeper structures of the eye are often involved in the pathogenic process. Thus imaging of the sclera and retrobulbar structures could be very useful for diagnosis and follow-up of these conditions.

The best imaging techniques to study the pathology of deep structures such as retrobulbar neoformations, posterior scleritis, and macular bucklings currently include ultrasonography (USG) and magnetic resonance imaging (MRI).[11,12] Unfortunately, the highest resolution of these techniques is around 100 μm in the axial plane (standard 20 MHz USG probe for eye and orbit examination).[13] Considering that in a previous report the mean (±standard deviation) choroidal thickness in healthy subjects was equal to 287 ± 74 μm,[7] it is clear that USG and MRI can successfully resolve only major changes in these tissues. In contrast, SD-OCT images have an axial resolution of 7 to 8 μm and a transverse resolution of 14 μm. Thus it can detect even minimal differences in thickness or composition of the posterior structures of the eye. Consequently, it represents the best choice for the study of these tissues during the diagnostic process and for monitoring the effectiveness of therapeutic intervention.[14]

EDI-OCT can image the deeper structures of the eye better than standard OCT. The visualization of these structures, including the sclera, was reported to be easier in myopic eyes than in emmetropic eyes.[8] Detailed images of the tissues that lie beyond the sclera have been described only in a few myopic subjects.[15] The explanation of this can be found in the different factors that affect EDI-OCT signal strength and, as a consequence, the capability of visualizing ocular deeper structures. The aim of this study was to identify these factors.

Materials and Methods

This study followed the tenets of the Declaration of Helsinki and was approved by the local ethics committee. Informed consent was obtained from the enrolled subjects. Thirty consecutive eyes from 21 patients were selected for the study. The inclusion criterion was a spherical equivalent refractive error of 6 diopters (D) or more of myopia. Exclusion criteria included choroidal neovascularization, chorioretinal atrophy, scars, or any other pathological condition affecting the posterior pole.

Each patient underwent slit-lamp examination, visual acuity examination, postpharmacological cycloplegic autorefraction (ARK900; Nidek, Gamagori, Japan), and noncontact biometry (Lenstar LS900; Haag-streit AG, Koeniz, Switzerland) to assess axial length. Irises were classified as lightly (blue, green) or darkly (brown) pigmented. Spectral-domain OCT scans were obtained with the Heidelberg Spectralis (Heidelberg Engineering, Heidelberg, Germany). Seven sections, each composed of 100 averaged scans, were obtained in a 5° × 30° area encompassing the macula and optic nerve. Imaging was done with and without the EDI function activated. The scan obtained without the EDI function was used to assess the central retinal thickness while the EDI-OCT scans were used to analyze the choroid, the sclera, and the structures beyond the sclera.

Heidelberg Spectralis software (Eye Explorer 1.6.4.0; Heidelberg Engineering) was used to obtain and analyze the OCT scans. During standard examinations, the software performed automated analysis using an algorithm to segment the layers by identifying, according to brightness changes across the image, the inner limiting membrane and Bruch's membrane. The software then generated retinal thickness values after determining the distance between these structures.

Operators were allowed to correct automatic segmentation artifacts by manually shifting the lines drawn by the software. Because the thickness values generated by the automated analysis correspond to the vertical distance between the two segmentation lines, manual segmentation was also used to measure other posterior pole structures. In particular we obtained choroidal thickness values by manually moving the segmentation lines to encompass the inner and outer border of the choroid. After this procedure, choroidal thickness values were automatically generated by the software (Fig. 1).

Choroidal thickness was assessed in all eyes. Measurements were performed on the horizontal section passing through the center of the fovea. We analyzed 13 segments of choroidal thickness. The central segment was under the fovea, and the others were located at 500-μm intervals extending 3 mm nasally and temporally.

In eyes with a fully visible sclera, the thickness was calculated using the same technique as for the choroid. The measurement procedure for both the choroid and sclera was repeated by two different operators to test for reproducibility. The ability to visualize structures beyond the sclera was also assessed.

Statistical Analysis

Statistical analysis was performed using R language (R Development Core Team, http://www.R-project.org, accessed May 20, 2012). Means and standard deviations for refractive error, axial length, choroidal thickness, and mean scleral thickness were calculated. The frequency of cases in which the entire sclera was visible and in which the retrobulbar structures could be visualized was assessed. For statistical analysis, patients in which the posterior limit of the sclera was not visible by EDI-OCT were designated as group 1. Patients in which the sclera was fully visible by EDI-OCT were designated as group 2.

The factors that influenced the visualization of the sclera were tested by a multifactorial regression analysis using a generalized linear model (GLM) for binomial variables (logit). This analysis was computed by comparing the visualization of the sclera as the independent variable with the refractive error, axial length, pigmentation of the iris, mean retinal thickness, and mean choroidal thickness as dependent variables. For patients in which the sclera was entirely visible (group 2), the factors that influenced the visualization of the retrobulbar structures (independent variable) were evaluated by the same statistical test with the refractive error, axial length, pigmentation of the iris, mean retinal thickness, mean choroidal thickness, and mean scleral thickness as dependent variables. Reproducibility was tested with paired *t*-tests.

Results

The mean age of the patients (16 women and 5 men) was 47.0 ± 16.9 (range, 23–74) years. All patients showed good visual acuity (mean: 20/20), except for one eye that was amblyopic, whose best-corrected visual acuity was 20/63. There were 22 eyes with darkly pigmented irises. The mean spherical equivalent was −11.26 ± 4.01 D, and the axial length was 28.28 ± 1.20 mm. Measurements of choroidal and scleral thickness were highly reproducible ($P = 0.2$ and 1.0, respectively) between the two independent observers. The mean central retinal thickness was 271.5 ± 24.3 μm.

The choroid was visible and the thickness measurable in all eyes. The subfoveal mean choroidal thickness was 133.2 ± 102 μm. In 11 eyes the sclera was not completely visualized (group 1, Figs. 2A, 2B) while in 19 eyes the full scleral thickness was measured (group 2, Figs. 2C–F, Table 1). Choroidal thickness gradually increased from the peripapillary area to the temporal region 3 mm from the fovea (Fig. 3A).

Iris pigmentation, axial length, refraction, and central retinal thickness were not significantly different between

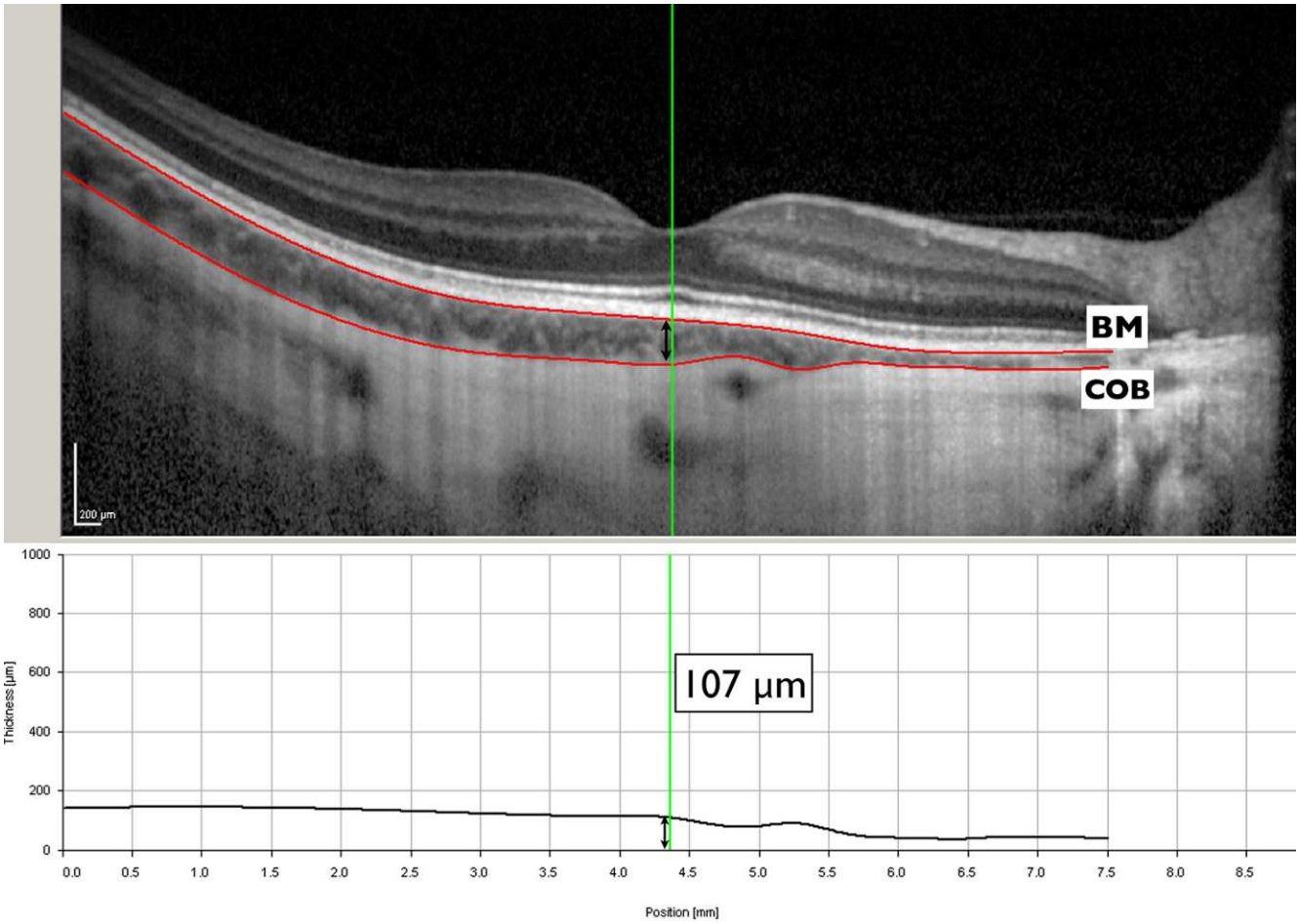

Figure 1. Technique for measuring choroidal thickness. To assess retinal thickness, the software automatically set the segmentation lines corresponding to Bruch's membrane (BM) and the inner limiting membrane. To evaluate choroidal thickness, the inner reference segmentation line was manually shifted to the BM corresponding to the inner limit of the choroid, while the outer one was placed to encompass the outer border of the choroid (COB). Thickness values, measured as the distance in micrometers between the two segmentation lines, were automatically generated by the software and displayed in the graph in the lower part of the image. The *green vertical line* in the OCT image could be moved by the operator to show the corresponding thickness value. In this example, the software displays subfoveal choroidal thickness (*black double-headed arrow*), corresponding to 107 µm (thickness value displayed by the software is enlarged in the picture).

group 1, in which the full scleral thickness was not visible, and group 2, in which it was ($P > 0.05$ for each, Table 1). However, the choroidal thickness in group 1, 205.6 ± 58 µm, was significantly greater ($P < 0.001$), than in group 2, 68.42 ± 29.88 µm (Table 1). Thus only choroidal thickness was correlated with the ability to visualize scleral thickness.

The scleral thickness in group 2 subjects did not follow a specific pattern of changes along the posterior pole (Fig. 3B). The mean scleral thickness was 309.10 ± 65.44 µm. In 7 out of the 19 eyes of group 2, the full sclera was the deepest structure detected (group 2A, Figs. 2C–D). In the other 12 eyes of group 2, deeper structures were visualized beyond the sclera (group 2B, Figs. 2E–F, Table 2).

Iris pigmentation, axial length, refraction, central retinal thickness, and scleral thickness were not significantly different between group 2A, in which the retrobulbar structures were not visible, and group 2B, in which they were ($P > 0.05$ for each, Table 2). However, the choroidal thickness in group 2A, 97.73 ± 16.24 µm, was significantly greater ($P = 0.044$), than in group 2B, 51.32 ± 21.25 µm (Table 2). Thus only choroidal thickness was correlated with the ability to visualize the retrobulbar structures.

Discussion

To ensure the passage of light with no abnormal impediments, we enrolled only myopic eyes with good visual acuity and no pathological alterations of the retina or the overlying layers.[1,16] Thus, we were able to measure retinal thickness, choroidal thickness, and where visible, scleral thickness. Choroidal thickness increased gradually from the nasal to the temporal region. This is consistent with the findings of Fujiwara et al.[8] in highly myopic eyes.

Scleral thickness variations across the posterior pole in myopic eyes were previously studied by Makuru et al.[17] using a high-penetration prototype OCT. The authors reported that the subfoveal thickness was around 300 µm, which is consistent with our findings that the mean scleral thickness in group 2 (patients with visible full scleral thickness) was 309.14 ± 65.43 µm. Makuru et al.[17] also found the sclera to be thicker in the subfoveal area compared with the rest of the posterior pole. This feature was not confirmed by our findings. According to our results, scleral thickness did not follow a specific pattern of variation across the posterior pole. The reasons for this discrepancy could be explained by the different scan patterns used in the two studies. Compared with Makuru et al.,[17] we collected more measurements, and

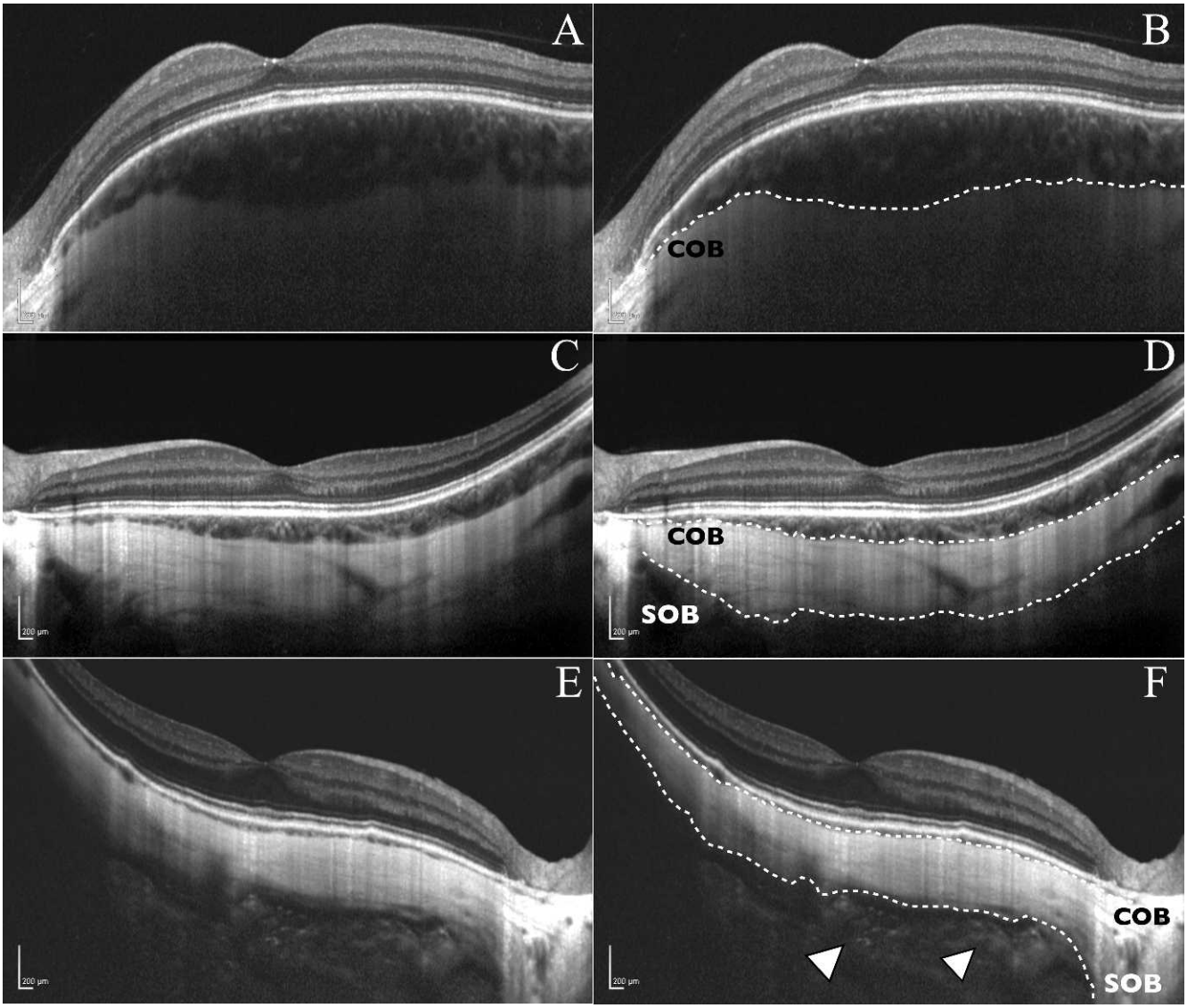

FIGURE 2. EDI-OCT in three myopic patients, without (**A**, **C**, **E**) and with (**B**, **D**, **F**) segmentation lines. COB, choroidal outer boundaries; SOB, scleral outer boundaries; *white arrowheads*: retrobulbar structures. (**A**, **B**) Scan from a patient in group 1. Posterior limits of the choroid were detected and segmented (**B**). The limits of the sclera were not visible due to EDI-OCT signal attenuation. (**C**, **D**) Scan from a patient in group 2A. Both choroidal and scleral outer boundaries were detected and segmented (**D**). Full scleral thickness was visualized, but the deeper structures were not clearly visible. (**E**, **F**) Images of a patient in group 2B. Both choroidal and scleral outer boundaries were detected and segmented (**F**). Tissues beyond the sclera were clearly detected in the nasal part of the scan (*arrowheads*).

they were on a single line from the nasal to the temporal region, encompassing the fovea. In contrast, Makuru et al.[17] evaluated the scleral thickness in all four quadrants of the posterior pole, but they used only single measurements, each of which was 3 mm from the fovea. For this reason, and considering the small sample size of our study population, further studies are needed before our results on scleral thickness variations across the posterior pole can be considered valid for myopic eyes in general. Moreover it has to be considered that all thickness measurements were assessed on the vertical axis. This choice was made because the principal aim of the study was to analyze the factors influencing OCT

TABLE 1. Structural Properties of All Study Eyes*

Property	Group 1 ($n = 11$)	Group 2 ($n = 19$)	P
Dark iris	8/11	14/19	0.106
Choroidal thickness	205.6 ± 58 μm	68.42 ± 29.88 μm	<0.001
Axial length	27.42 ± 1.09 mm	28.78 ± 0.97 mm	0.729
Refraction	−8.86 ± 1.80 D	−12.65 ± 4.30 D	0.484
Central retinal thickness	279.27 ± 24.56 μm	267 ± 23.64 μm	0.769

* Group 1, posterior limit of the sclera not visible by EDI-OCT; group 2, full thickness sclera visible by EDI-OCT. *P* values indicate levels of significance in comparisons between groups 1 and 2. Continuous variables presented as means ± standard deviations.

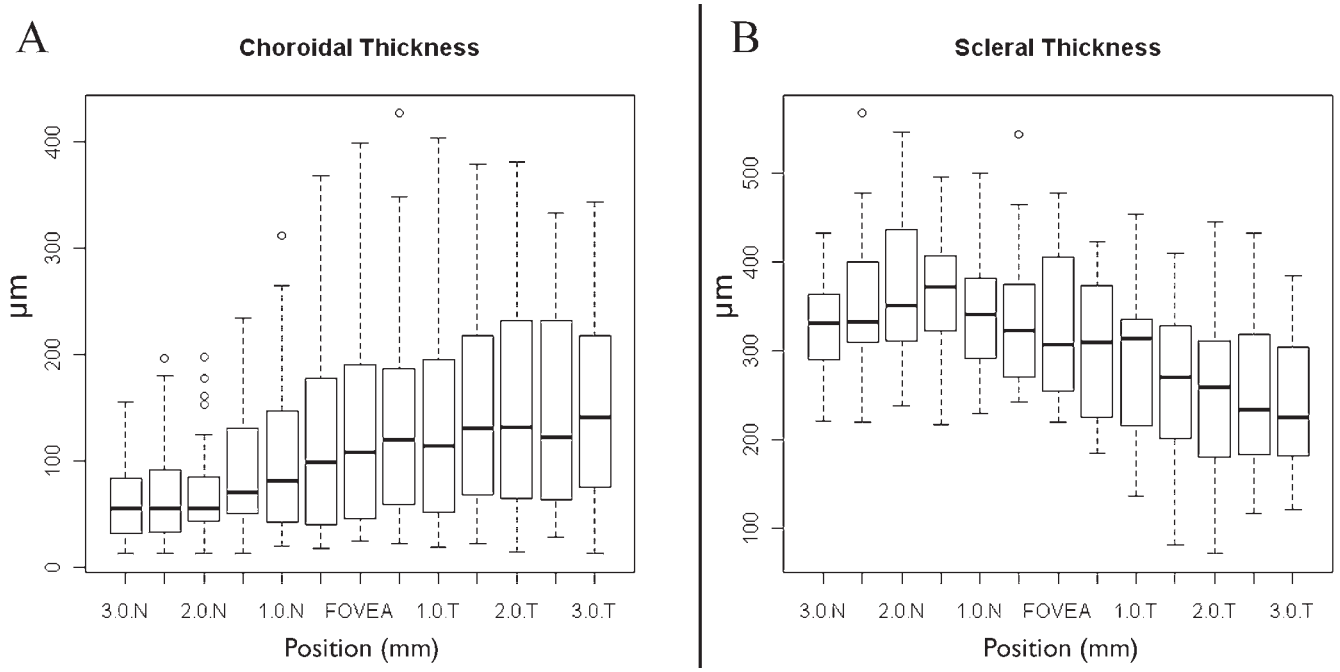

Figure 3. Thickness measurement variations across the posterior pole. Measurements for the choroid (**A**) and sclera (**B**) were made from 3.0 mm nasally to 3.0 mm temporally, passing through the fovea. N, nasal; T, temporal.

signal attenuation. However, in the extreme temporal and nasal parts of the scan the angulation of structures increases. This may lead to an exaggeration of thickness measurements in the periphery that should be taken into account.

The thickness of the central retina did not appear to be a factor in the visualization of the full sclera or the retrobulbar structures. This is not a surprising result because of the transparency of this tissue and the absence of alterations such as fibrotic scars or exudates that could have blocked the EDI-OCT signal. In contrast, the correlation between choroidal thickness and the visualization of the full sclera was statistically significant. For eyes in which the sclera was fully visible, the thickness was calculated using the same method as for the choroid.

Scleral thickness did not have any impact on retrobulbar imaging. This was probably due to the homogeneous composition of the sclera. Collagenous fibers within this layer are interwoven in an irregular and complex pattern that gives the sclera its typical rigid-elastic consistency and at the same time a very compact texture.[18] This organization results in the absence of density changes that could absorb or scatter the OCT signal within this layer and could explain the good permeability of the sclera to the OCT light. Only choroidal thickness determined the ability to visualize retrobulbar structures. Even though data from this study are not sufficient to completely explain this finding we may hypothesize some particular characteristics of the choroid to play a relevant role. First, the choroidal vasculature is not a homogeneous structure; rather it is composed of many elements such as blood, vessels walls, connective tissue, and interstitial spaces of different densities. Moreover these components are randomly arranged, increasing the number of interfaces that the EDI-OCT signal passes through. All of these elements can cause light scattering.[16,19] Additionally, moving elements such as blood cells within the vessels of the choroid, also contribute to increased light scattering.[20]

Another important role could be played by the amount of pigmentation of the choroid. Melanin within the choroid absorbs part of the EDI-OCT light, thus decreasing penetration.[21,22] Iris color has been used as an indirect estimate of choroidal pigmentation[23]; however, in our study we found that the presence of dark or light irises did not influence the ability of EDI-OCT to visualize retrobulbar structures. A possible explanation may be that in the multifactorial analysis of factors that determine the visualization of retrobulbar structures, choroidal thickness plays a much greater role than does iris (or choroidal) pigmentation. It is likely that in patients with equivalent choroidal thickness, the pigmentation influences the visualization of retrobulbar structures. However, the sample size of this study is not sufficient to execute such a stratified analysis.

Table 2. Structural Properties of Group 2 Eyes*

Property	Group 2A ($n = 7$)	Group 2B ($n = 12$)	P
Dark iris	3/7	11/12	0.545
Choroidal thickness	97.73 ± 16.24 µm	51.32 ± 21.25 µm	0.044
Axial length	28.11 ± 0.79 mm	29.17 ± 0.87 mm	0.820
Refraction	−10.57 ± 2.94 D	−13.87 ± 4.60 D	0.729
Central retinal thickness	260.86 ± 24.72 µm	270.58 ± 23.31 µm	0.605
Scleral thickness	356.30 ± 51.01 µm	281.62 ± 57.84 µm	0.106

* Group 2A, retrobulbar structures not visible by EDI-OCT; group 2B, retrobulbar structures visible by EDI-OCT. P values indicate levels of significance in comparisons between groups 2A and 2B. Continuous variables presented as means ± standard deviations.

Investigative Ophthalmology & Visual Science

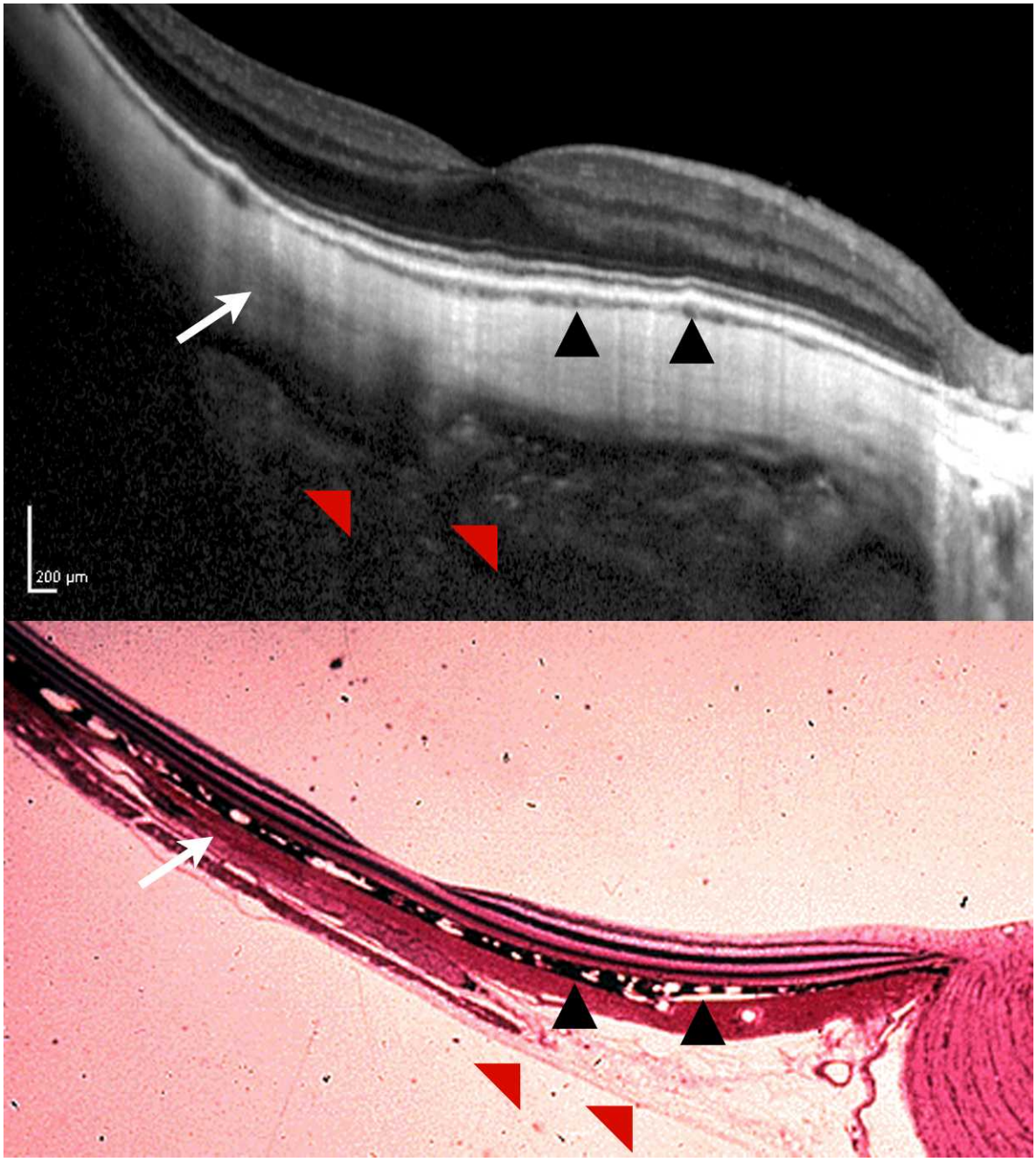

FIGURE 4. Comparison between EDI-OCT imaging and histological imaging. The EDI-OCT image (**A**) and the histological section of a healthy human eye stained with a hematoxylin-eosin (**B**) showed the choroid (*black arrowheads*) and the sclera (*white arrows*). The EDI-OCT image visualized retrobulbar structures (*red arrowheads*) that may correspond to adipose tissue in the histological section (*red arrowheads*). The histological section is reprinted with permission of University of Delaware.

According to literature posterior structures of the eye were better visualized in myopic eyes.[8,15] This suggests a possible positive correlation between the refractive error and the image quality. Moreover, an inverse correlation between axial length and choroidal thickness has been described.[8] Since in this study choroidal thickness influenced the visualization of retrobulbar structures, we expected the axial length to also have an influence. However, neither refractive error nor axial length showed any impact on EDI-OCT visualization of retrobulbar structures. This apparent incongruence is probably due to the presence of some outliers in the study population that showed a thick choroid even with an axial length of 29 mm or more.

The nature of the retrobulbar structures that can be visualized in some patients remains uncertain. Comparison with histological sections from human donors suggests that these structures may correspond to retrobulbar adipose tissue (Fig. 4). Additional studies focused on specific pathologies (e.g., scleritis or retrobulbar infiltrative processes) may help to better understand this issue and may suggest the clinical relevance of these findings.

In conclusion, EDI-OCT is a suitable technique to image the deep structures of the myopic eye. With this imaging modality, the only limiting element in the visualization of full scleral thickness and retrobulbar tissues is the thickness of the

choroid. Further studies are needed to confirm these data and provide useful information for the improvement of this technique. These data may also help in the development of new instruments capable studying in detail the posterior sclera and tissues beyond it.

Acknowledgments

The authors thank Sara Bochicchio, MD, for helping with data analysis.

The authors alone are responsible for the content and writing of the paper.

Disclosure: **A. Invernizzi**, None; **A. Giani**, None; **M. Cigada**, None; **G. Staurenghi**, Heidelberg Engineering (C)

References

1. Drexler W, Fujimoto JG. State-of-the-art retinal optical coherence tomography. *Prog Retin Eye Res*. 2008;27:45–88.
2. Gabriele ML, Wollstein G, Ishikawa H, et al. Optical coherence tomography: history, current status, and laboratory work. *Invest Ophthalmol Vis Sci*. 2011;52:2425–2436.
3. Mojana F, Cheng L, Bartsch DU, et al. The role of abnormal vitreomacular adhesion in age-related macular degeneration: spectral optical coherence tomography and surgical results. *Am J Ophthalmol*. 2008;146:218–227.
4. Ishida S, Nishizawa N. Quantitative comparison of contrast and imaging depth of ultrahigh-resolution optical coherence tomography images in 800–1700 nm wavelength region. *Biomed Opt Express*. 2012;3:282–294.
5. Povazay B, Hofer B, Torti C, et al. Impact of enhanced resolution, speed and penetration on three-dimensional retinal optical coherence tomography. *Opt Express*. 2009;17:4134–4150.
6. Spaide RF, Koizumi H, Pozzoni MC. Enhanced depth imaging spectral-domain optical coherence tomography. *Am J Ophthalmol*. 2008;146:496–500.
7. Margolis R, Spaide RF. A pilot study of enhanced depth imaging optical coherence tomography of the choroid in normal eyes. *Am J Ophthalmol*. 2009;147:811–815.
8. Fujiwara T, Imamura Y, Margolis R, Slakter JS, Spaide RF. Enhanced depth imaging optical coherence tomography of the choroid in highly myopic eyes. *Am J Ophthalmol*. 2009;148:445–450.
9. Wong IY, Koizumi H, Lai WW. Enhanced depth imaging optical coherence tomography. *Ophthalmic Surg Lasers Imaging*. 2011;42(suppl): S75–S84.
10. Fong A, Li K, Wong D. Enhanced depth imaging spectral domain optical coherence tomography in Vogt-Koyanagi-Harada disease. *Retina*. 2011;31:502–509.
11. Platnick J, Crum AV, Soohoo S, Cedeno PA, Johnson MH. The globe: infection, inflammation, and systemic disease. *Semin Ultrasound CT MR*. 2011;32:38–50.
12. Okhravi N, Odufuwa B, McCluskey P, Lightman S. Scleritis. *Surv Ophthalmol*. 2005;50:351–363.
13. Coleman D, Silverman R, Chabi A, et al. High-resolution ultrasonic imaging of the posterior segment. *Ophthalmology*. 2004;111:1344–1351.
14. Erdol H, Kola M, Turk A. Optical coherence tomography findings in a child with posterior scleritis. *Eur J Ophthalmol*. 2008;18:1007–1010.
15. Imamura Y, Iida T, Maruko I, Zweifel SA, Spaide RF. Enhanced depth imaging optical coherence tomography of the sclera in dome-shaped macula. *Am J Ophthalmol*. 2011;151:297–302.
16. Wang RK. Signal degradation by multiple scattering in optical coherence tomography of dense tissue: a Monte Carlo study towards optical clearing of biotissues. *Phys Med Biol*. 2002;47:2281–2299.
17. Makuru I, Iida T, Sugano Y, Oyamada H, Akiba M, Sekiryu T. Morphologic analysis in pathologic myopia using high-penetration optical coherence tomography. *Invest Ophthalmol Vis Sci*. 2012;53:3834–3838.
18. Komai Y, Ushiki T. The three-dimensional organization of collagen fibrils in the human cornea and sclera. *Invest Ophthalmol Vis Sci*. 1991;32:2244–2258.
19. van Velthoven ME, Faber DJ, Verbraak FD, van Leeuwen TG, de Smet MD. Recent developments in optical coherence tomography for imaging the retina. *Prog Retin Eye Res*. 2007;26:57–77.
20. Kalkman J, Bykov AV, Streekstra GJ, van Leeuwen TG. Multiple scattering effects in Doppler optical coherence tomography of flowing blood. *Phys Med Biol*. 2012;57:1907–1917.
21. Hu DN, Simon JD, Sarna T. Role of ocular melanin in ophthalmic physiology and pathology. *Photochem Photobiol*. 2008;84:639–644.
22. Jacob D, Shelton RL, Applegate BE. Fourier domain pump-probe optical coherence tomography imaging of melanin. *Opt Express*. 2010;18:12399–12410.
23. Keilhauer CN, Delori FC. Near-infrared autofluorescence imaging of the fundus: visualization of ocular melanin. *Invest Ophthalmol Vis Sci*. 2006;47:3556–3564.

Investigative Ophthalmology & Visual Science